



## A new optical-based technique for real-time measurements of mineral dust concentration in PM<sub>10</sub> using a virtual impactor

5 Authors: Luka Drinovec<sup>1</sup>, Jean Sciare<sup>2</sup>, Iasonas Stavroulas<sup>2</sup>, Spiros Bezantakos<sup>2</sup>, Michael Pikridas<sup>2</sup>, Florin Unga<sup>2</sup>,  
Chrysanthos Savvides<sup>3</sup>, Bojana Višić<sup>1,4</sup>, Maja Remškar<sup>1</sup>, Griša Močnik<sup>1,5</sup>

<sup>1</sup>Jozef Stefan Institute, Ljubljana, Slovenia

<sup>2</sup>Climate and Atmosphere Research Center, The Cyprus Institute, Nicosia, Cyprus

10 <sup>3</sup>Ministry of Labour and Social Insurance, Department of Labour Inspection, Nicosia, Cyprus

<sup>4</sup>Institute of Physics Belgrade, University of Belgrade, Belgrade, Serbia

<sup>5</sup>Center for Atmospheric Research, University of Nova Gorica, Ajdovščina, Slovenia

Keywords: mineral dust, aerosol absorption, virtual impactor, PM<sub>10</sub>

15

Correspondence to: luka.drinovec@ijs.si

20

**Abstract.** Atmospheric mineral dust influences Earth's radiative budget, cloud formation and lifetime, has adverse health effects, and affects the air quality through the increase of regulatory PM<sub>10</sub> concentrations, making strategic its real-time quantification in the atmosphere. Only few near-real-time techniques can discriminate dust aerosol in PM<sub>10</sub> samples and they are based on the dust chemical composition. The on-line determination of mineral dust using aerosol absorption photometers offers an interesting and competitive alternative, but remains a difficult task to achieve. This is particularly challenging when dust is mixed with black carbon, which features a much higher mass absorption cross-section. We present here for the first time a highly time resolved on-line detection technique of dust absorption by coupling a high flow virtual impactor (VI) sampler that concentrates coarse particles with an aerosol absorption photometer (Aethalometer, model AE33). The absorption of concentrated dust particles is obtained by subtracting the absorption of the submicron (PM<sub>1</sub>) aerosol fraction from the absorption of the virtual impactor sample (VI-PM<sub>1</sub> method). This real-time method for detecting desert dust was tested in the field for a period of two months (April and May 2016) at a regional background site of Cyprus, in the Eastern Mediterranean. Several intense desert mineral dust events were observed during the field campaign with dust concentration in PM<sub>10</sub> up to 45 μg m<sup>-3</sup>. Mineral dust was present most of the time during the campaign with an average PM<sub>10</sub> of about 8 μg m<sup>-3</sup>. Mineral dust absorption was most prominent at short wavelengths, yielding an average mass absorption cross-section (MAC) of 0.24 ± 0.01 m<sup>2</sup> g<sup>-1</sup> at 370 nm and an absorption Ångström exponent of 1.41 ± 0.29. This MAC value can be used as site specific parameter for on-line determination of mineral dust concentration. The uncertainty of the proposed method is discussed by comparing and validating it with different methods.

45



## 1. Introduction

50 Atmospheric dust often dominates  $PM_{10}$  aerosol mass concentrations in many regions of the world, and is the  
second most abundant aerosol source at a global scale just after sea spray. Its lifetime in the atmosphere is  
similar to carbonaceous aerosols (Boucher et al., 2013). Dust particles modify the Earth's radiation balance as  
they absorb and scatter light, affecting regional climate and precipitation regimes. The net radiative effect of  
atmospheric dust depends on the interplay between the heating of the atmosphere, due to the increased  
55 absorption of sunlight, and cooling due to scattering of sunlight back into space leading to a direct radiative  
forcing of dust estimated around  $-0.1 \pm 0.2 \text{ W m}^{-2}$  (Myhre et al., 2013). Dust deposits on snow and ice increase  
the ion content in snow and snow water (Greilinger et al., 2018) and they exert a warming influence after  
deposition (Di Mauro et al., 2015). Desert dust impacts industrial production to a degree that has been  
fictionalized (Herbert, 1965) and Saharan dust events have been shown to increase morbidity and have  
60 negative influence on health mainly through respiratory and cardiovascular effects (Middleton et al., 2008;  
Perez et al., 2012). The health effects of mineral dust are being considered in the context of regulation (WHO,  
2018).

Dust particles are often transported from the Sahara over the Mediterranean and southern Europe and can  
contribute significantly to mass concentration of particles smaller than  $10 \mu\text{m}$  in diameter –  $PM_{10}$  (Rodriguez et  
al., 2001; Vrekoussis et al., 2005). Mineral dust is considered as natural aerosol within the European Air Quality  
65 Directive (2008/50/EC) and, as such, can be subtracted from the daily (24h)  $PM_{10}$  reported by EU member  
states, potentially reducing the number of days with  $PM_{10}$  exceedances (European Commission, 2011).

Daily time resolution of the described method has been validated with the chemical composition and positive  
matrix factorization (Viana et al., 2010). Methods with higher temporal resolution have the potential to bring  
70 considerably more detail and information to the analysis of dust in  $PM_{10}$ . These methods capture the temporal  
variability dependent on the synoptic conditions more accurately; they allow the discrimination of long-range  
transported dust from locally resuspended one (by traffic as an important example); they provide considerably  
more detail to constrain chemistry-transport models; and can be used in real-time to inform the public and  
stakeholders and therefore improve adaptation measures. The higher time resolution requires use of novel and  
75 innovative approaches and instrumentation.

There are several sampling devices, which allow for hourly or sub-hourly sampling of ambient dust aerosols,  
such as Streaker sampler, the DRUM (Davis Rotating-drum Unit for Monitoring) sampler (Bukowiecki et al.,  
2005; Visser et al., 2015) and the SEAS (Semi-continuous Elements in Aerosol Sampler) (Chen et al., 2016). Mass  
80 loadings of trace metals collected by these samplers can be analyzed with high sensitive accelerator-based  
analytical techniques. However, a major drawback of these analyses is that they require a large commitment of  
analytical resources and time. Recent technical developments have been developed for more precise, accurate  
and frequent measurement of ambient metal species, such as XactTM 625 automated multi-metals analyzer  
(Fang et al., 2015; Jeong et al., 2016; Phillips-Smith et al., 2017; Cooper et al., 2010).

85 Dust scatters and absorbs light and its optical properties have been used in on-line measurements to derive the  
wavelength dependence of the single scattering albedo (SSA) (parameterized with the Ångström exponent) as  
the criterion to characterize Saharan dust events in the high Alpine region (Collaud Coen et al., 2004). The  
impact of Saharan dust events, showing increased absorption and scattering, was determined in the East  
90 Mediterranean (Vrekoussis et al., 2005) and the West Mediterranean (Pandolfi et al., 2011; Pandolfi et al.,  
2014; Ealo et al., 2016). These measurements with high time resolution have shown that the optical properties  
can be used to identify dust events but have not been able to determine the contribution of desert dust to  
 $PM_{10}$  concentrations in a quantitative manner based on the dust absorption.

95 Few studies have reported the potential of using dust aerosol absorption properties to infer their ambient  
concentrations in  $PM_{10}$ . These efforts started by using Aethalometers to determine the absorption coefficient  
attributed to iron compounds in dust, the determination of their mass absorption cross section, and the  
determination of black carbon and dust in the marine boundary layer (Fialho et al., 2005; Fialho et al., 2006;  
Fialho et al., 2014). The absorption of dust was due to iron compounds which were quantified using  
100 instrumental neutron activation analysis. Zhang et al. (2008) used thermal-optical reflection to measure the  
carbonaceous fraction and proton induced X-ray emission for elemental analysis, and again used iron as the  
dust tracer to separate the contributions of these two light-absorbing aerosol components. These publications



105 systematically biased the absorption coefficients too high due to the assumption that the attenuation of light in  
the filter is due to non-filter-enhanced absorption, neglecting the enhancement due to the scattering in the  
filter matrix. Using different influence of iron-containing mineral dust and black carbon on SSA at different  
wavelengths and contrasting fine and coarse fractions, Derimian et al. (2008) quantified the iron  
concentrations in mineral dust. Lately, more sophisticated techniques using filter photometers were employed  
to determine the mineral dust absorption coefficients, mass absorption cross-sections and dust SSA. Caponi et  
al. (2017) used the multi-wavelength absorbance analyzer to determine the absorption coefficients at multiple  
110 wavelengths and obtain the absorption Ångström exponents and mass absorption cross-sections in a chamber  
study. The chamber study was also used to determine the filter enhancement in Aethalometers challenged  
with dust (Di Biagio et al., 2017) and then use these parameters to determine the optical properties as a  
function of iron content for different dust samples from all over the world (Di Biagio et al., 2019).

115 Additionally, quantitative determination of ambient concentration of mineral dust has been performed in the  
mixture of Saharan dust and carbonaceous matter in a wildfire plume (Schauer et al., 2016). These two may be  
internally mixed (Hand et al., 2010). The relationship between the columnar optical properties and the in-situ  
ones during dusty and dust-free days due to the mixing of the dust with the dominant local air pollution is  
challenging to interpret (Valenzuela et al., 2015).

120 The determination of the optical absorption of pure mineral dust - when mixed with black carbon - is more  
difficult because black carbon features a much higher mass absorption cross-section, obscuring the smaller  
contribution of dust to absorption. Enriching the aerosol coarse fraction, and hence increasing the contribution  
of weakly absorbing dust, may represent an innovative alternative way to increase dust aerosol absorption  
125 relative to black carbon.

We present here an improvement in real-time detection of mineral dust in ambient *PM* by concentrating the  
coarse particle fraction with a high-volume virtual impactor system similar to the one reported by Sioutas et al.  
(1994), and coupled with an aerosol absorption monitor (Aethalometer model AE33). We demonstrate its  
130 performance at a regional background site, frequently impacted by Saharan dust.

First the enhanced absorption of coarse particles is determined from the difference of absorption measured by  
Aethalometers with the virtual impactor and  $PM_{10}$  inlet, respectively. This parameter is divided by the  
enhancement factor calculated from the particle size distributions, yielding the absorption of coarse particles.  
135 The correlation between mineral dust absorption and reference mineral dust concentration provides us with  
the mass absorption cross-section of the mineral dust, which is then used to determine mineral dust  
concentration with high time resolution.

## 140 2. Materials and methods

### 2.1. Field campaign site description

Field validation took place at the Cyprus Atmospheric Observatory (CAO) between 1 April 2016 and 31 May  
2016. This field campaign was organized as part of the European projects ACTRIS (Aerosols, Clouds and Trace  
145 Gases Research Infrastructure) and BACCHUS (Impact of Biogenic versus Anthropogenic emissions on Clouds  
and Climate; towards a Holistic UnderStanding). CAO is situated at a regional background site on the foothills of  
mount Troodos (35.04N; 33.06E; 535 m a.s.l.) in the centre of Cyprus, an island located in the Eastern  
Mediterranean - Levantine basin. Lying in close proximity to the Middle-East/North Africa (MENA) region,  
Cyprus is often influenced by air masses carrying mineral dust particles, originating from either the Saharan  
Desert or the Middle East (Mamouri et al., 2013; Pikridas et al., 2018). During this field campaign, a large suite  
150 of in-situ and remote sensing instrumentation was deployed at ground level and onboard Unmanned Aerial  
Vehicles in order to better characterize the influence of desert dust on Ice Nuclei (Schrod et al., 2017; Marinou  
et al., 2019), LIDAR retrieval of vertically-resolved *PM* (Mamali et al., 2018), and performance of miniaturized  
light absorption sensors (Pikridas et al., 2019). More information on the climatology of air masses origin and  
155 *PM* at the Cyprus Atmospheric Observatory can be found in Pikridas et al., 2018).



## 2.2. Instrumentation

160 Real-time aerosol absorption of the dust-containing coarse fraction was determined by subtracting aerosol  
absorption of black carbon-containing submicron aerosols from the absorption of the concentrated coarse  
aerosols from the outlet of a virtual impactor (VI). A detailed description of this instrumental set-up as well as  
complementary aerosol instrument is provided in the following.

### 2.2.1. Virtual Impactor design

165 Based on a design similar to the one reported by Sioutas et al. (1994), our virtual impactor is sampling ambient  
air (TSP) at a total flow rate of  $100 \text{ l min}^{-1}$ . The major flow ( $F_{in} = 98 \text{ l min}^{-1}$ ) is carried out of the VI by a large  
capacity pump while the coarse particles are inertially impacted (enriched) into the minor flow ( $F_{out} = 2 \text{ l min}^{-1}$ )  
170 of the VI connected to the absorption photometer. The enrichment of coarse particles in the minor flow is a  
function of the ratio of the two (major/minor) flows; its efficiency depends also on the design and  
manufacturing of the VI. For that reason, the VI was thoroughly tested and characterized in the lab in order to  
estimate the concentration enhancement (CE) factor of coarse particles as a function of particle size (using NIST  
polystyrene-latex (PSL) spheres with nominal sizes from  $0.7$  to  $10 \mu\text{m}$ ) and two different flow rate ratios ( $19$   
175 and  $50$ , respectively). The laboratory characterisation of the VI is described in the Supplement S1 while the  
methodology used to reconstruct the size distribution of concentrated coarse particles (in the minor flow  $F_{out}$ )  
is presented in section 3.1.

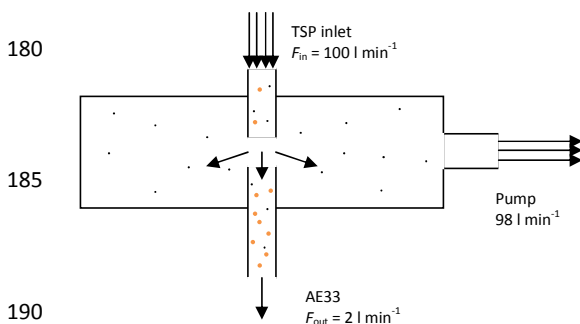


Figure 1. Principle of the Virtual Impactor (VI) operation.

### 2.2.2. Aerosol absorption and light scattering coefficients

195 Three Aethalometers model AE33 (Magee Scientific, USA) were used during the field campaign with different  
inlet setups: one sampling through a PM1 sharp-cut cyclone (BGI Inc., Model SCC 1.197), one sampling through  
a custom-made total suspended particles (TSP) inlet and a third one sampling through the VI described above  
(Section 2.2.1). The first two instruments (with PM1 and TSP) were sampling at a  $5 \text{ l min}^{-1}$  flow rate, while the  
third was sampling through the VI at a  $2 \text{ l min}^{-1}$  flow rate. This flow rate of  $2 \text{ l min}^{-1}$  was selected so as to  
200 increase concentration enhancement (CE) factor of the VI and consequently increase the absorption signal of  
dust aerosols.

The Aethalometer AE33 measures attenuation of light by two samples collected at different flow rates. This  
results in two sample spots that feature different attenuation values. The measurement of light transport  
205 through the sample-laden filter is non-linear and the measurements using two sample spots allow the on-line  
compensation of the nonlinearity of the black carbon measurement (Drinovec et al., 2015). Given that the on-  
line filter loading compensation was not working efficiently for the AE33 coupled with the virtual impactor (see  
section 3.3, below), the obtained data was compensated using fixed  $k$  values as described in the Supplement  
S2.

210



Absorption coefficient ( $b_{\text{abs}}$ ) was calculated from the attenuation coefficient ( $b_{\text{atn}}$ ) using the value of the multiple scattering parameter  $C$  of 2.6:

$$215 \quad b_{\text{abs}} = \frac{b_{\text{atn}}}{C} \quad (1)$$

This value was derived from the value obtained for quartz filter: 3.5 (WMO, 2016) instead of 2.14 used previously (Weingartner et al., 2003) and adjusted for the AE33 filter (Drinovec et al., 2015) to 2.6 instead of 1.57. The  $\sigma_{\text{air}}$  value for black carbon was adjusted in the inverse manner to obtain the same BC values; new mass absorption cross section for BC  $\sigma_{\text{air}}$  at 880 nm is now  $4.74 \text{ m}^2 \text{ g}^{-1}$  instead of  $7.77 \text{ m}^2 \text{ g}^{-1}$ :

$$220 \quad BC = \frac{b_{\text{abs}}}{\sigma_{\text{air}}} = \frac{b_{\text{atn}}}{C \cdot \sigma_{\text{air}}} \quad (2)$$

The Aethalometers were intercompared in the laboratory before the campaign. The correlation slope for 1 minute resolution data differed less than 4% between the instruments with  $R^2 = 0.996$ . The analysis of the actual uncertainty of Aethalometer measurements during the campaign is presented in the Supplement S3.

Total scattering and back-scattering coefficients ( $b_{\text{scat}}$  &  $b_{\text{bscat}}$ ) of the ambient (TSP) aerosol were monitored continuously using a three-wavelength (450, 550 and 700 nm) integrated nephelometer (TSI Inc., model 3563; Anderson and Ogren, 1998). The nephelometer was sampling through a vertical, straight sampling line, coupled with a TSP inlet, a Nafion dryer, and measuring at 1-minute time resolution. Calibration was conducted using  $\text{CO}_2$  as a high, and zero air as a low span gas prior to the field campaign. This nephelometer went through a successful inter-comparison exercise at the European Center for Aerosol Calibration (ECAC-report-IN-2015-1-5, 2016) ahead of the instrument's field deployment. Nevertheless, due to miscalibration of the green channel, 550 nm measurements were excluded from the analysis. Single scattering albedo (SSA) was calculated at 450 and 700 nm using the total scattering coefficient from nephelometer and absorption coefficient obtained from AE33 by linear interpolation of absorption coefficients from adjacent wavelength pairs. Single scattering albedo Ångström exponent (SSAAE) was calculated from  $\text{SSA}_{450 \text{ nm}}$  and  $\text{SSA}_{700 \text{ nm}}$ .

### 240 2.2.3. Other in-situ aerosol instrumentation

Dried particle number size distributions (PNSDs) were measured using a TSI Inc. Aerodynamic Particle Sizer (APS, model 3321). The APS measures PNSDs in the  $0.5 - 20 \mu\text{m}$  aerodynamic diameter size range at a 5-minute temporal resolution. The APS was sampling at a total flow rate of  $5 \text{ l min}^{-1}$  through a straight vertical sampling line, a Nafion dryer, and a TSP inlet, identical to the nephelometer. Aerosol mass concentration for fine ( $PM_{2.5}$ ) and coarse aerosols ( $PM_{10-2.5}$ ) was measured using a Continuous Dichotomous Ambient Particulate Monitor (Thermo Scientific, 1405-DF TEOM-FDMS system) deployed at the Agia Marina Xyliatou EMEP station, collocated with CAO, at a 1-hour temporal resolution (see more at Pikridas et al., 2019).

## 250 2.3. Filter sampling and analysis

### 2.3.1 Filter sampling

Aerosol samples were collected during the field campaign at a flow rate of  $2.3 \text{ m}^3 \text{ h}^{-1}$  on pre-weighed filters (Pall Tissuquartz 2500 QAT-UP) using two autonomous filter samplers (Leckel SEQ 47/50) for determination of mass concentration ( $PM_{2.5}$  and  $PM_{10}$ , respectively) with 24-h time resolution from midnight to midnight according to local standard time. Particle mass concentration ( $PM_{2.5}$  and  $PM_{10}$ ) on the filter substrates was determined gravimetrically before and after the sampling, under constant conditions dictated by protocol EN12341 with the use of a 6 digits precision analytical balance (Mettler Toledo, Model XP26C). According to that protocol filters were subjected to 45-50% relative humidity at  $20 \pm 1^\circ \text{C}$  for 48 hours.



260 **2.3.2 Aerosol chemical mass closure**

Filter samples were subsequently analyzed for major ions by ion chromatography (Thermo, Model ICS5000) following the protocol reported in Sciare et al. (2011) and complying with the European committee for standardization for the measurement of anions and cations in PM<sub>2.5</sub> (EN 16913:2017) and elemental carbon concentration (EC) and organic carbon concentration (OC) with a Sunset Lab Instrument, the EUSAAR\_2 thermo-optical protocol (Cavalli et al., 2010) and complying with the European committee for standardization (EN 16909:2017). Quality of ion measurements is checked at the bi-annual intercomparison studies performed in the framework of the EMEP and WMO networks while quality of EC/OC measurements is confirmed on annual basis in the framework of ACTRIS network.

265  
270 Estimation of dust in PM<sub>2.5</sub> and PM<sub>10</sub> was performed following the methodology proposed by Sciare et al. (2005) for a regional background (Crete Island) located in the Eastern Mediterranean assuming a constant Calcium-to-dust ratio of 0.12. Reconstruction of PM from chemical analyses versus PM from gravimetry is reported in Supplement S6 and shows very good correlation ( $R^2 = 0.99$ ) and slope close to one, supporting the consistency and robustness of our calculation of mineral dust in PM.

275

**2.3.3 Trace metal analysis using inductively coupled plasma mass spectrometry (ICP-MS)**

An acid microwave digestion procedure was applied to the PM<sub>10</sub> filters followed by inductively coupled plasma mass spectrometry (ICP-MS, Thermo Electron X Series) to measure metal concentrations of Al, V, Cr, Mn, Fe, Ni, Cu, Zn, Cd, and Pb, following the procedure from Poulakis et al. (2015).

280

**2.3.4 Scanning electron microscopy – energy dispersive X-ray (SEM-EDX) analysis**

Scanning electron microscopy measurements were performed at Jožef Stefan Institute using SEM model Supra 35 VP (Carl Zeiss, Germany). Measurements were performed on punches of PM10 filters that were attached to the sample holder through a double-sided carbon tape. The filters were previously sputter-coated with a thin gold film (with Au nanoparticle approximate size of 10 nm) using an SCD 005 cool sputter coater (BAL-TEC GmbH, Leica Microsystems, Wetzlar, Germany). The microscope was equipped with the energy dispersive spectroscopy module (EDX, Oxford INCA 400, Oxford Instruments Analytical, UK), which was operated at an accelerating voltage of 20 kV.

285

290

**2.4. Data coverage**

The measurement campaign took place in April and May 2016. Due to technical reasons not all of the instruments were running throughout the campaign (Table 1). This limited some of the analysis to a shorter time periods with most of the data available between 14 April and 6 May.

295

**Table 1. Data coverage for on-line instrumentation and filter sampling.**

Instrument	Available data
AE33	4 Apr 2016 – 31 May 2016
VI	14 Apr 2016 – 6 May 2016
TEOM-FDMS	1 Apr 2016 – 31 May 2016
Nephelometer	14 Apr 2016 – 31 May 2016
APS	1 Apr 2016 – 30 Apr 2016
24h filter samples	1 Apr 2016 – 31 May 2016



300 **3. Results and discussion**

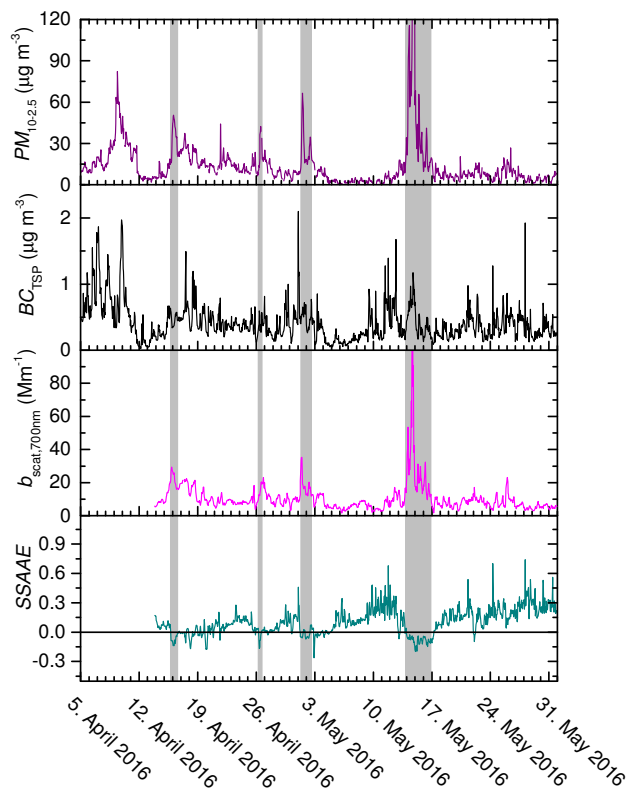
The methodology to derive real-time concentration of dust in  $PM_{10}$  is presented as per the follow: the robustness of the system (VI+AE33) is tested first in the field for a period of 1 month in Section 3.1. The enhancement factor (EF) downstream of the virtual impactor is calculated in Section 3.2. Real-time absorption of ambient dust aerosols is calculated in section 3.3. It is corrected for 1) the influence of Black Carbon measured by a co-located Aethalometer AE33 equipped with  $PM_1$  inlet, and 2) the Enhancement Factor of the VI. Real-time dust concentration of  $PM_{10}$  (Section 3.4) is then derived by dividing the absorption of dust aerosols calculated in section 3.3 with a Mass Absorption Cross-section (MAC) for dust calculated using filter-based chemical analyses.

310

**3.1. Field campaign overview**

Optical, physical, and size-resolved chemical properties of ambient aerosols at the Cyprus Atmospheric Observatory were characterised continuously in April and May 2016 using several online and offline methods as illustrated in Figure 2. During the campaign a total of four intense events (16 and 26 April, 1 and 15 May 2016) were detected with increased  $PM$  concentration of the coarse fraction concurrent with increase of the light scattering coefficient, but no correlation with black carbon concentration (Figure 2). By combining light absorption and scattering measurements it is possible to identify the mineral dust events as the periods during which the single scattering albedo Ångström exponent (SSAAE) becomes negative, indicating the presence of mineral dust (Collaud Cohen et al., 2004).

320



325 **Figure 2.** Time series of the mass concentration of coarse particles ( $PM_{10-2.5}$ ) obtained by TEOM-FDMS, black carbon concentration (BC) for total suspended particles (TSP) obtained by Aethalometer AE33, the light scattering coefficient at 700 nm obtained by nephelometer and Single scattering albedo Ångström exponent (SSAAE). The four periods with negative SSAAE during the campaign are shadowed.



Figure 3 reports continuous measurements of aerosol absorption during the field campaign for three different aerosol size fractions that were achieved using different inlets for three Aethalometers AE33 running in parallel: 1) a  $PM_{10}$ ; 2) a total suspended particle (TSP), and 3) a virtual impactor (VI). During the first days of the campaign, the VI was operated manually for several periods of few hours in order to perform several tests related to the collection and light absorption detection of the coarse fraction. The VI was set ON continuously from 14<sup>th</sup> April till 6<sup>th</sup> May. Given the strong sensitivity of dust aerosol absorption in the UV range compared to black carbon (see Section 3.3), the 370 nm channel was selected here to compare aerosol absorption measurements from the three Aethalometers.

As shown in Figure 3 the absorption in TSP is closely related to the one of  $PM_{10}$ . On contrary, the absorption measured when the virtual impactor was ON shows very high values and very poor correlation with the other absorption measurements. During the periods when the VI pump was not operating, the aerosol absorption agrees well with the one using the TSP showing that the enhancement of aerosol absorption is entirely related to the enhancement of the coarse fraction

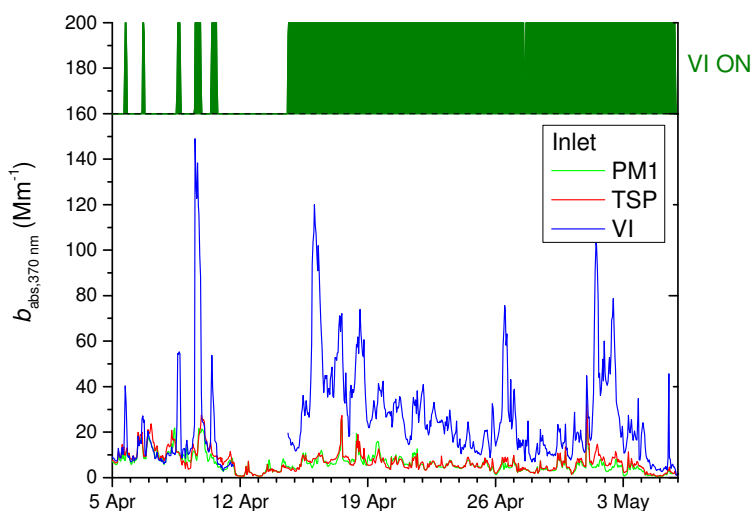
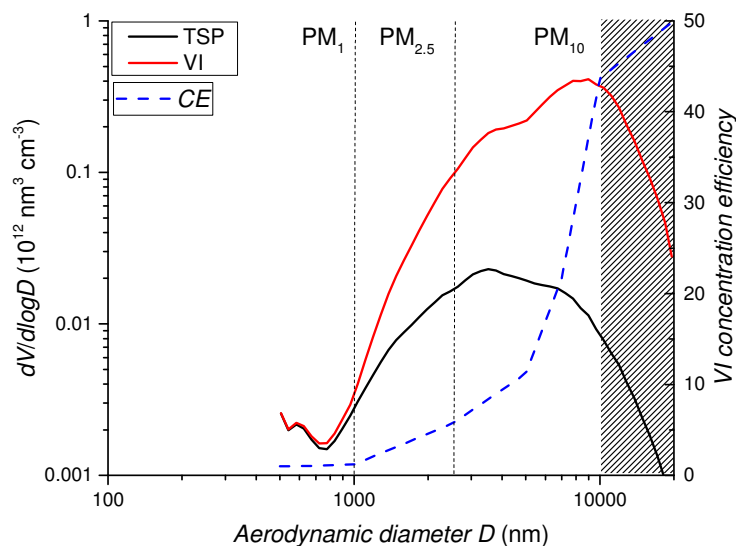


Figure 3. Time series of the aerosol absorption coefficient at 370 nm for three Aethalometers AE33 running in parallel and equipped with different inlets:  $PM_{10}$ , total suspended particle (TSP) and virtual impactor (VI). The periods when VI was operating are marked in green (VI=ON).

### 3.2. Experimental characterization of the enhancement factor of coarse particles using the virtual impactor

The performance of the virtual impactor was characterised during the laboratory campaign (Supplement S1). The maximum concentration efficiency was obtained for  $F_{in}/F_{out}$  ratio of 50 (Table S1). Therefore, a similar  $F_{in}/F_{out}$  ratio of 50 was chosen during the field deployment with  $F_{in}$  of  $100 \text{ l min}^{-1}$  and  $F_{out}$  of  $2 \text{ l min}^{-1}$ , respectively. As shown in Table S1 for  $F_{in}/F_{out}$  ratio of 50, the concentration efficiency (CE) of aerosols with diameters of  $1 \mu\text{m}$  and below is close to unity. This result is expected for a virtual impactor which principle is based on the concentration of large aerosols. Consequently, the black carbon fraction – mainly located in the submicron mode – is not enriched in the VI. On contrary, dust aerosols - mostly located in the coarse aerosol fraction (above  $1 \mu\text{m}$  diameter) are concentrated efficiently by the virtual impactor (Figure 4).



360 **Figure 4. Average aerodynamic volume size distribution spectrum measured by APS between 1 April 2016 – 30 April 2016 (black line) and the predicted spectrum of aerosol concentrated using the virtual impactor (red line). Blue line represents the virtual impactor concentration efficiency measured in laboratory (Supplement S1). Shaded area denotes the particles larger than 10  $\mu\text{m}$ .**

The enhancement factor (*EF*) of the VI is defined as a multiplication factor that reflects the enrichment of the coarse fraction downstream of the VI. *EF* was determined experimentally during the field test using the Aerodynamic Particle Sizer (APS) to derive both the volume concentration of the unperturbed sample (*V*) and volume concentration enhanced using a virtual impactor (*V<sub>VI</sub>*):

$$V = \int \left( \frac{dV}{d \log D} \right) * d \log D \quad , \quad (3)$$

370 
$$V_{VI} = \int \left( \frac{dV}{d \log D} \right) * CE * d \log D \quad , \quad (4)$$

where *D* is the particle aerodynamic diameter and *CE* the collection efficiency of the VI as characterized in supplement S1. The enhancement factor is then calculated as:

375 
$$EF = \frac{V_{VI}}{V} \quad . \quad (5)$$

The average aerosol volume concentration size spectrum obtained during the campaign by the APS is presented in Figure 4 (black line), along with the spectrum calculated for the virtual impactor (red line), using the concentration efficiency determined during the laboratory campaign (Table S1). For ambient aerosol we observe a mode around 3.5  $\mu\text{m}$ . Because the virtual impactor is more efficient towards larger particles, the ambient volume size distribution is not reproduced downstream of the VI, which shows a maximum around 9  $\mu\text{m}$ . The collection efficiency of particles larger than 10  $\mu\text{m}$  in the Aethalometer AE33 downstream the VI is expected to be rather low due to losses in tubing and sample lines inside the Aethalometer. Overall, the uncertainty associated with the enhancement factor remains difficult to assess in the aerosol range close to 10  $\mu\text{m}$  diameter which particles are usually difficult to collect in a quantitative way.

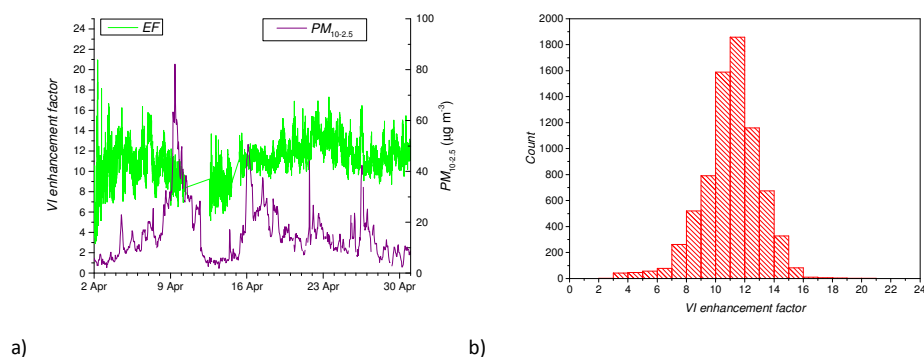
380  
385



390 The enhancement factor of the VI defined in Eq. 5 depends on the ambient aerosol volume size distribution  
 measured by the APS, which changes over time. Figure 5 reports the temporal variation of  $EF$  during the field  
 campaign at 5 min time resolution. There are time intervals with stable  $EF$  of approximately 9 (11 April 2016 –  
 13 April 2016), also we can observe some peaks with  $EF$  as high as 16. For the  $PM_{10}$ - $PM_1$  particles we obtained  
 a campaign average VI enhancement factor:

$$EF = 11 \pm 2.$$

395



400 **Figure 5.** Time series of the virtual impactor enhancement factor calculated from aerodynamic size distributions  
 measured by APS (a) for the  $PM_{10}$  aerosol fraction. The enhancement factor frequency distribution is shown on the right  
 (b).

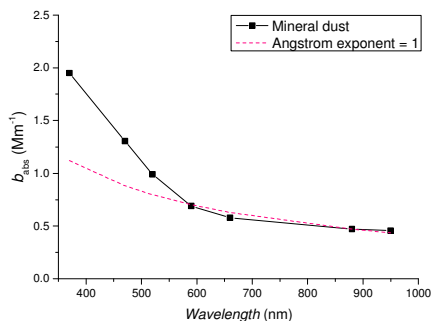
### 3.3. Calculation of the absorption coefficient of coarse particles

405 The principle of the virtual impactor operation allows for concentration of the coarse particles while the fine  
 particles remain present at the same amount as in the ambient air. To determine the absorption induced by  
 ambient mineral dust, we need to subtract the fine particle absorption signal (dominated by black carbon) from  
 the total virtual impactor absorption and normalize by the enhancement factor, following the equation:

$$410 \quad b_{abs,mineral\ dust} = \frac{b_{abs,VI} - b_{abs,PM1}}{EF}, \quad (6)$$

where  $b_{abs,mineral\ dust}$ ,  $b_{abs,VI}$  and  $b_{abs,PM1}$  represent absorption coefficients of dust in ambient conditions, aerosols  
 downstream of the virtual impactor and submicron aerosols, respectively. Because absorption of  $PM_1$  fraction  
 is dominated by black carbon, it is essential to compensate absorption data for the filter loading effect  
 415 (Drinovec et al., 2017). If the compensation parameter is wrong by 0.005 this can result in over- or under-  
 estimation of  $b_{abs}$  by up to 60% at 370 nm and by 25% at 950 nm. For the Aethalometer with the  $PM_1$  inlet, the  
 absorption data is sufficiently compensated by the built-in dual-spot algorithm. For the Aethalometer  
 connected to the virtual impactor, the method was not able to measure accurately the loading effect due to  
 the presence of coarse particles (Supplement S2). The main reason for this behaviour lies in the fact that a  
 420 single particle (deposited on one of the two spots) potentially causes significant absorption only in one of the  
 two measurement spots. This requires an application of off-line compensation using fixed values of the  
 compensation parameters (Supplement S2).

425 The absorption induced by dust (Eq. 6) during the field campaign was calculated for each of the 7 wavelengths  
 of the Aethalometer AE33 and averaged, as shown in Figure 6. The spectral dependence of absorption by  
 mineral dust shows an increase at shorter wavelengths, significantly deviating from the Ångström exponent of  
 1. The best discrimination between the mineral dust particles and black carbon is achieved at the lowest  
 wavelength 370 nm, which is the wavelength that has been selected in our procedure to derive the absorption  
 and the atmospheric concentration of mineral dust.



430 **Figure 6. Averaged absorption coefficient during the campaign for ambient dust (as calculated in Eq. 6) in the coarse**  
 435 **fraction of aerosols as calculated from the difference of the absorption coefficients measured with a virtual impactor and**  
 440 **a PM<sub>1</sub> inlet, and divided by the average enhancement factor (black line). The dotted red line shows a theoretical curve**  
 445 **with Ångström exponent of 1, extrapolated from measurements at 880 nm.**

435 Campaign averages show the mean value for absorption at 370 nm being higher for TSP compared to PM<sub>1</sub> inlet  
 (Table 2). The absorption signal reported in this table for the AE33 behind the VI is more than a factor of 4  
 higher compared to AE33 with the PM<sub>1</sub> inlet and is due to the concentrated mineral dust in the coarse fraction.  
 440 The average absorption coefficient of ambient dust as calculated using Eq. 6 was  $2.0 \pm 2.1 \text{ Mm}^{-1}$ . Similarly to  
 absorption, AAE shows higher value for TSP compared to PM<sub>1</sub> inlet, as the mineral dust in the coarse fraction  
 increases absorption in UV & blue part of the spectrum. As expected there is high variability both for  
 absorption and AAE during the campaign. The average difference between absorption for TSP and PM<sub>1</sub> inlets is  
 445 lower than expected, but within the measurement variation and uncertainty - the  $b_{\text{abs},370\text{nm}}$  measurements  
 were affected by the uncertainty up to 18% during the campaign (as estimated comparing Aethalometers with  
 different inlets, Supplement S3).

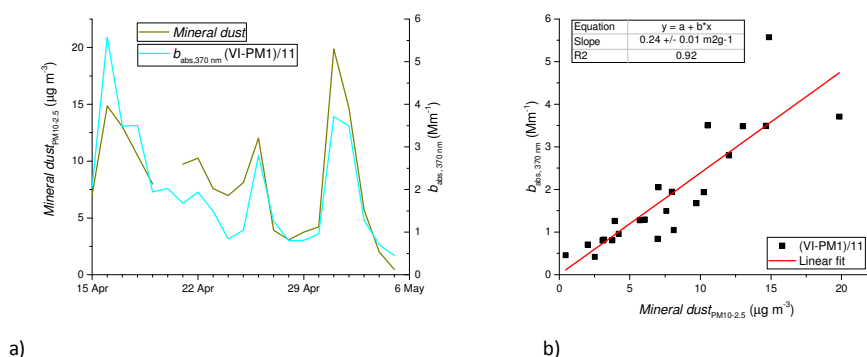
450 **Table 2. Average absorption coefficient at 370 nm, the absorption Ångström exponent (AAE) and their variation between**  
**during the campaign (15 April 2016 and 6 May 2016). AAEs were calculated as averages of one hour values for the**  
**wavelength pair of 370 and 950 nm.**

Sample	$b_{\text{abs},370\text{nm}} \text{ (Mm}^{-1}\text{)}$	AAE
PM1	$5.6 \pm 3.3$	$1.22 \pm 0.16$
TSP	$6.1 \pm 3.4$	$1.30 \pm 0.18$
VI	$27.6 \pm 20.1$	$1.38 \pm 0.25$
VI-PM1	$22.0 \pm 23.4$	$1.41 \pm 0.29$
(VI-PM1)/11	$2.0 \pm 2.1$	$1.41 \pm 0.29$



### 3.4. Determination of mineral dust mass absorption cross-section

455 For the determination of the mineral dust mass absorption cross-section, we need to establish the mineral dust  
 concentration in our samples. For this purpose, we performed mass closure on 24-hour PM<sub>10</sub> and PM<sub>2.5</sub> filter  
 samples (see Supplement S6). Mineral dust concentration was determined from calcium concentration,  
 assuming 12% Ca in mineral dust. Since the virtual impactor concentrates larger particles with higher efficiency  
 (this is where we expect to have the largest contribution of mineral dust), we used the coarse fraction PM<sub>10-2.5</sub>  
 460 for the calibration (Figure 8).



a) b)  
**Figure 8. The time-series (a) and the correlation (b) between the absorption coefficient of coarse particles obtained using VI-PM1 method versus mineral dust concentration in the coarse fraction.**

465 The correlation between mineral dust absorption and filter measurements is very good with R<sup>2</sup> of 0.92 showing  
 good agreement between the methods. The mineral dust mass absorption cross-section was obtained from the  
 regression between mineral dust mass and the coarse fraction absorption coefficient at 370 nm:

470

$$MAC_{\text{mineral dust},370\text{nm}} = 0.24 \pm 0.01 \text{ m}^2 \text{ g}^{-1}.$$

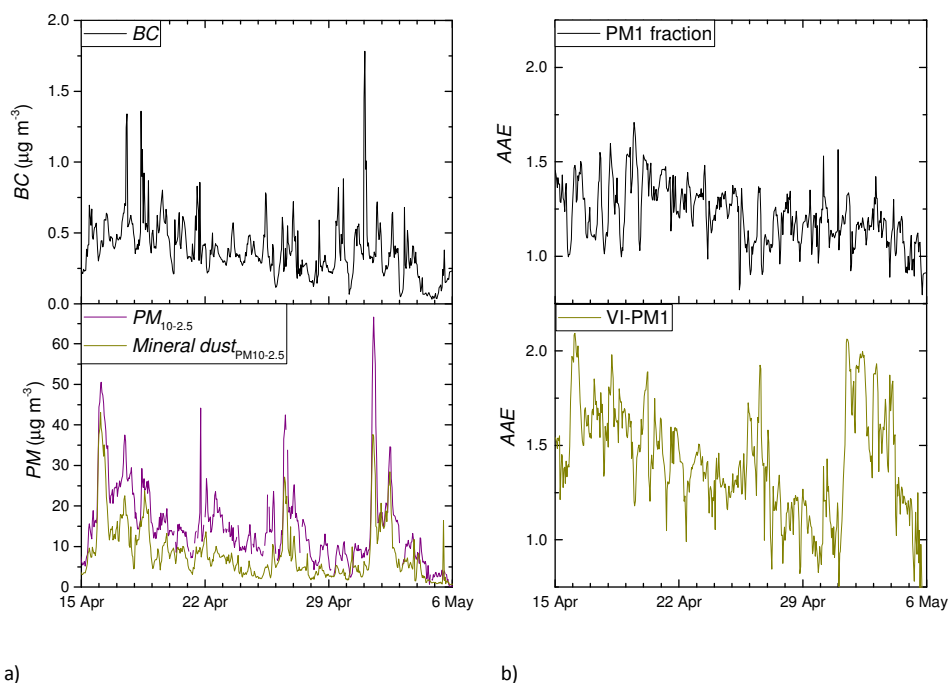
This MAC value, obtained with 24-h time resolution, allows us to calculate mineral dust concentrations with the  
 high time resolution of the absorption measurements:

475

$$\text{Mineral dust}_{\text{PM}_{10-2.5}} = \frac{(b_{\text{abs},370\text{nm,VI}} - b_{\text{abs},370\text{nm,PM1}})}{EF \cdot MAC_{\text{mineral dust},370\text{nm}}} \quad (7)$$

480 The concentration of coarse particles and its composition show a huge variability during the campaign (Figure  
 9a): the average mineral dust concentration was 8.1 µg m<sup>-3</sup> with peaks up to 45 µg m<sup>-3</sup>. On average, mineral  
 dust represented about one half of the coarse fraction. The average BC was much lower at 0.39 µg m<sup>-3</sup>. Due to  
 its much higher mass absorption cross-section (MAC<sub>BC,370nm</sub> = 11.2 m<sup>2</sup> g<sup>-1</sup>; 47 times higher compared to mineral  
 dust), the absorption of black carbon dominated the aerosol absorption in Cyprus during the campaign and  
 mineral dust absorption could not be detected directly. Using the virtual impactor allows us to concentrate the  
 dust and measure its absorption coefficient and determine its mass absorption cross-section with a low  
 485 uncertainty.

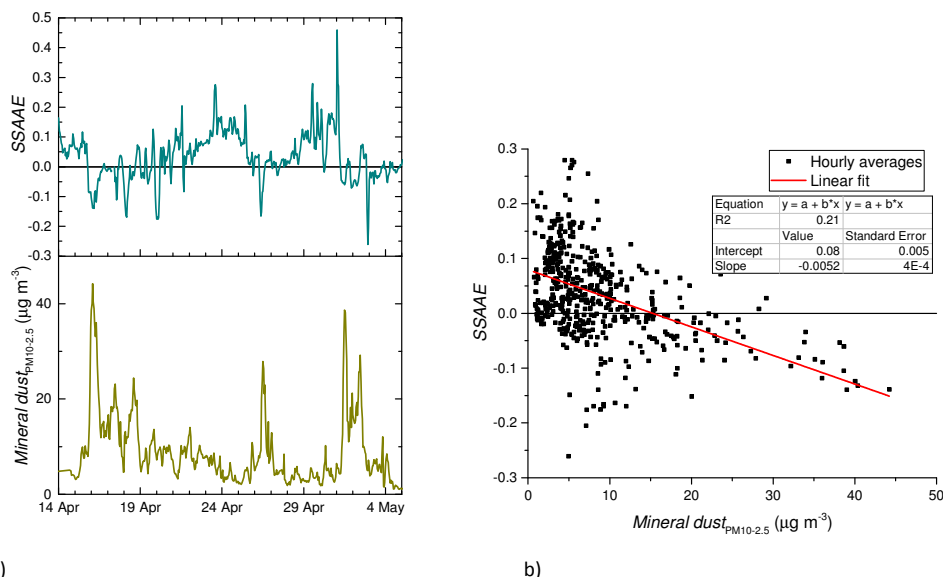
490 The Ångström exponent of the fine fraction oscillates between 1 and 1.5 (Figure 9b). The lower values  
 correspond to BC peaks, originating from local traffic and other efficient combustion sources. The higher values  
 are a mixture of mineral dust and local pollution. The Ångström exponent of the coarse fraction reaches value  
 of 2.1 during intense mineral dust periods. After these events the AAE value drops slowly and reaches a value  
 of 1.2 during the period with low presence of mineral dust (around 27 April 2019 – 1 May 2019).



495

**Figure 9. Time series of BC in fine fraction and mineral dust determined using VI-PM1 method (a) and Ångström exponent for fine and coarse fraction of the aerosol (b).**

500 The knowledge of the virtual impactor enhancement factor allowed us to calculate the average MAC for  
mineral dust during the Cyprus campaign. Reportedly, its value depends mostly on the absorption of iron  
oxides (Sokolik and Toon, 1999, Alfaro et al., 2003; Fialho et al., 2005; Fialho et al., 2006; Fialho et al., 2014;  
Caponi et al., 2017; Di Biagio et al., 2019). During the campaign we obtained 1.9% iron in  $\text{PM}_{10}$ . If we take into  
account that mineral dust represented about one half of  $\text{PM}_{10}$  (Supplement S6), we get a good agreement with  
iron concentrations measured for mineral dust from Middle East of 3.15% – 3.5% (Linke et al., 2006), 3.8% - 5%  
505 (Caponi et al., 2017) and Sahara of 3.6% - 6.6% (Caponi et al., 2017). Surprisingly our  $\text{MAC}_{\text{Mineral dust}, 370\text{nm}} = 0.24$   
 $\text{m}^2 \text{g}^{-1}$  is much larger compared to mineral dust from Saudi Arabia of  $0.09 \text{ m}^2 \text{g}^{-1}$ , Libya of  $0.089 \text{ m}^2 \text{g}^{-1}$  and  
Algeria of  $0.099 \text{ m}^2 \text{g}^{-1}$  (Caponi et al., 2017) or North-Eastern Africa of  $0.099 \text{ m}^2 \text{g}^{-1}$  (Fialho et al., 2006). Higher  
MAC goes along with the low Ångström exponent value of 2.1 obtained for the fresh mineral dust reaching  
Cyprus. This value is lower than AAE of 2.8 – 4.1 reported for Middle East (2.8 – 4.1) and Sahara (2.5 – 3.2) by  
510 Caponi et al. (2017) or 2.9-4 for North-Eastern Africa (Fialho et al., 2005; Fialho et al., 2006). Differences in MAC  
values and the Ångström exponent can be an indicator that the coarse fraction of mineral dust is contaminated  
with black carbon, with the mixing occurring in or close to the source regions much earlier than mineral dust  
reached Cyprus.



515 a)

b)

**Figure 10. Time-series (a) and correlation (b) of the single scattering albedo Ångström exponent (SSAAE) and mineral dust concentration.**

520 The determination of the mineral dust concentration was tested using the Collaud Coen et al. (2004) method for the qualitative determination of Saharan dust events. As expected the peaks in mineral dust concentration correspond to the periods featuring negative values of single scattering albedo Ångström exponent. It is shown (Figure 10) that SSAAE becomes negative when the mineral concentration becomes larger than  $15 \mu\text{g m}^{-3}$ . The correlation between the mineral dust (determined from the chemical composition, notably calcium ions) and SSAAE is not perfect because of the contribution to scattering from other aerosol components (organics, sulphates ...) which amount to about one half of the aerosol mass, and the absorption of organics. While the SSAAE method provides an identification of dust events, the VI-PM1 method allows for the quantitative determination of mineral dust - even at high black carbon concentrations in the fine fraction.

### 530 3.7. Uncertainty of the VI-PM1 method for the determination of mineral dust concentrations in $PM_{10}$

The uncertainty in the determination of mineral dust concentration using VI-PM1 method arises from the measurement uncertainties, variability of optical and chemical properties of mineral dust and potential systematic biases of the method itself. Because VI-PM1 method is calibrated using mineral dust in the coarse fraction only, 6% lower values compared to total mineral dust in  $PM_{10}$  are reported. This bias can be avoided by using a correction factor.

The uncertainty of 10% in the determination of the attenuation coefficient at 880 nm by the Aethalometer AE33 was reported (Drinovec et al., 2015). The performance of the Aethalometers during this campaign was investigated by comparing signal from the instruments with TSP and  $PM_{10}$  inlets. The variation not related to the presence of mineral dust was used to determine measurement uncertainty of 11% and 880 nm and 18% at 370 nm (Supplement S4). The value of the multiple scattering parameter  $C$  (Weingartner et al., 2003; Drinovec et al., 2015; WMO, 2016) does not add to the final uncertainty because the same value is used for the calibration and the determination of mineral dust concentration, cancelling out in the final calculation. However, the selection of the parameter  $C$  influences the calculation of mineral dust absorption coefficient and  $MAC$ . Similar to parameter  $C$ , the selected value of  $EF$  influences determination of absorption coefficients and  $MAC$ , but not the calculation of mineral dust concentration. It is the variation of  $EF$ , caused by the changes of the particle size distribution (Figure 5a), which induces about 18% uncertainty.



550 The main uncertainty comes from the variability of the chemical composition, mainly from the variability of  
ratio of Fe/Ca. This ratio is important because  $MAC$  of mineral dust depends mostly on the iron content,  
whereas calcium was used as a reference method for determination of mineral dust concentration. The SEM-  
EDX analysis of single particle chemical composition show large particle-to-particle variation inside the 24 h  
filter sample (Supplement S8). As expected the day-to-day variability of chemical composition is much lower as  
555 shown by ICP-MS analysis of trace metals (Supplement S7) - we obtained 40% variability of Fe/Ca ratio both for  
the campaign period as for the year-long dataset.

The combined uncertainty in determination of mineral dust concentration during the Cyprus campaign  
assuming independent contributions is 44%. The main reason for this uncertainty is the variation of the  
560 measured parameters used for the calibration of the method, essentially “assuming the worst-case scenario” of  
ever-changing aerosolized dust composition and resulting in an overestimation of the uncertainty.  
Alternatively, it is possible to derive the uncertainty from the measurement accuracy: to compare daily mineral  
dust concentrations obtained using VI-PM1 method with the reference values obtained using mass closure.  
This compares different methods measuring the same sample. Standard deviation of the ratio between  
565 predicted and reference mineral dust concentration was 29%. This is a quantification of the scatter of the  
regression ( $R^2 = 0.92$ ) between the mineral dust concentrations determined using the two methods, as seen in  
Figure 8.

#### 570 4. Conclusions

- An on-line method (named VI-PM1) for the determination of mineral dust concentration in ambient  
air based on absorption of coarse particles was developed.
- 575 • The VI-PM1 method was calibrated using mass closure performed on 24h filter samples yielding the  
uncertainty between 29% and 44%, using measurement accuracy and variation of the measured  
parameters, respectively.
- The VI-PM1 method allows for easy quantification of mineral dust in environments, where dust  
absorption is otherwise masked by absorption by black carbon in the fine aerosol fraction.
- 580 • During the campaign, we observed a continuous presence of mineral dust with an average of  $8 \mu\text{g}/\text{m}^3$   
and several intense events with concentrations up to  $45 \mu\text{g m}^{-3}$ .
- An average  $MAC_{\text{mineral\_dust},370\text{nm}}$  of  $0.24 \pm 0.01 \text{ m}^2 \text{ g}^{-1}$  and Ångström exponent of  $1.41 \pm 0.29$  were  
obtained for mineral dust measured at a background location in Cyprus. This seems to indicate that  
coarse fraction might be contaminated by black carbon.

585 *Data availability.* Campaign data can be accessed at the data repository of the Cyprus Institute using the  
following link: <https://mybox.cyi.ac.cy/public.php?service=files&t=624a471bf356165df49cad6cc747b051>.

590 *Competing interests.* Luka Drinovec and Griša Močnik were, at the time of the campaign, but not analysis and  
writing of the manuscript, also employed by the manufacturer of the Aethalometer AE33 Aerosol d.o.o.  
(Slovenia). The methodology was protected with the patent application.

*Acknowledgements.* This work was supported by Slovenian research agency (grant BI-FR/CEA/15-17-004 and  
programme P1-0099), and Slovenian Ministry of Economic Development and Technology, project DNAAP.

595



## References

- Alfaro, S. C., Lafon, S., Rajot, J. L., Formenti, P., Gaudichet, A. and Maille', M.: Iron oxides and light absorption by pure desert dust: An experimental study. *J. Geophys. Res.*, 109, D08208, <https://doi.org/10.1029/2003JD004374>, 2004.
- 600 Anderson, T. L. and Ogren, J. A.: Determining Aerosol Radiative Properties Using the TSI 3563 Integrating Nephelometer, *Aerosol Science and Technology*, 29:1, 57-69, doi: 10.1080/02786829808965551, 1998.
- Boucher, O., Randall, D., Artaxo, P., Bretherton, C., Feingold, G., Forster, P., Kerminen, V.-M., Kondo, Y., Liao, H., Lohmann, U., Rasch, P., Satheesh, S.K., Sherwood, S., Stevens, B. and Zhang, X.Y.: Clouds and Aerosols. In: *Climate Change 2013: The Physical Science Basis. Contribution of Working Group I to the Fifth Assessment Report of the Intergovernmental Panel on Climate Change* [Stocker, T.F., D. Qin, G.-K. Plattner, M. Tignor, S.K. Allen, J. Boschung, A. Nauels, Y. Xia, V. Bex and P.M. Midgley (eds.)]. Cambridge University Press, Cambridge, United Kingdom and New York, NY, USA, 2013.
- 605 Bukowiecki, N., Hill, M., Gehrig, R., Zwicky, C. N., Lienemann, P., Hegedüs, F., Falkenberg, G., Weingartner, E., and Baltensperger, U.: Trace metals in ambient air: Hourly size-segregated mass concentrations determined by synchrotron-XRF, *Environ. Sci. Technol.*, 39, 5754–5762, <https://doi.org/10.1021/es048089m>, 2005.
- Caponi, L., Formenti, P., Massabó, D., Di Biagio, C., Cazaunau, M., Pangui, E., Chevaillier, S., Landrot, G., Andreae, M. O., Kandler, K., Piketh, S., Saeed, T., Seibert, D., Williams, E., Balkanski, Y., Prati, P., and Doussin, J.-F.: Spectral- and size-resolved mass absorption efficiency of mineral dust aerosols in the shortwave spectrum: a simulation chamber study, *Atmos. Chem. Phys.*, 17, 7175-7191, <https://doi.org/10.5194/acp-17-7175-2017>, 2017.
- 610 Cavalli, F., Viana, M., Yttri, K. E., Genberg, J., and Putaud, J.-P.: Toward a standardised thermal-optical protocol for measuring atmospheric organic and elemental carbon: the EUSAAR protocol, *Atmos. Meas. Tech.*, 3, 79–89, <https://doi.org/10.5194/amt-3-79-2010>, 2010.
- Chen, B., Stein, A. F., Castell, N., Gonzalez-Castanedo, Y., Sanchez de la Campa, A. M., and de la Rosa, J. D.: Modeling and evaluation of urban pollution events of atmospheric heavy metals from a large Cu-smelter, *Sci. Total Environ.*, 539, 17–25, <https://doi.org/10.1016/j.scitotenv.2015.08.117>, 2016.
- 620 Collaud Coen, M., Weingartner, E., Schaub, D., Hueglin, C., Corrigan, C., Henning, S., Schwikowski, M., and Baltensperger, U.: Saharan dust events at the Jungfraujoch: detection by wavelength dependence of the single scattering albedo and first climatology analysis, *Atmos. Chem. Phys.*, 4, 2465-2480, <https://doi.org/10.5194/acp-4-2465-2004>, 2004.
- 625 Cooper, J. A., Petterson, K., Geiger, A., Siemers, A., and Rupprecht, B.: Guide for developing a multi-metals, fenceline monitoring plan for fugitive emissions using X-ray based monitors, Cooper Environmental Services, Portland, Oregon, 1–42, , 2010.
- 630 Derimian, Y., Karnieli, A., Kaufman, Y. J., Andreae, M. O., Andreae, T. W., Dubovik, O., Maenhaut, W., and Koren, I.: The role of iron and black carbon in aerosol light absorption, *Atmos. Chem. Phys.*, 8, 3623–3637, <https://doi.org/10.5194/acp-8-3623-2008>, 2008.
- Di Biagio, C., Formenti, P., Balkanski, Y., Caponi, L., Cazaunau, M., Pangui, E., Journet, E., Nowak, S., Andreae, M. O., Kandler, K., Saeed, T., Piketh, S., Seibert, D., Williams, E., and Doussin, J.-F.: Complex refractive indices and single-scattering albedo of global dust aerosols in the shortwave spectrum and relationship to size and iron content, *Atmos. Chem. Phys.*, 19, 15503–15531, <https://doi.org/10.5194/acp-19-15503-2019>, 2019.
- 635 Di Biagio, C., Formenti, P., Cazaunau, M., Pangui, E., Marchand, N., and Doussin, J.-F.: Aethalometer multiple scattering correction Cref for mineral dust aerosols, *Atmos. Meas. Tech.*, 10, 2923–2939, <https://doi.org/10.5194/amt-10-2923-2017>, 2017.
- 640 Di Mauro, B., Fava, F., Ferrero, L., Garzonio, R., Baccolo, G., Delmonte, B. and Colombo, R.: Mineral dust impact on snow radiative properties in the European Alps combining ground, UAV, and satellite observations, *J. Geophys. Res. Atmos.*, 120, 6080–6097, <https://doi.org/10.1002/2015JD023287>, 2015.
- Drinovec, L., Gregorič, A., Zotter, P., Wolf, R., Bruns, E. A., Prévôt, A. S. H., Petit, J.-E., Favez, O., Sciare, J., Arnold, I. J., Chakrabarty, R. K., Moosmüller, H., Filep, A., and Močnik, G.: The filter-loading effect by ambient aerosols in filter absorption photometers depends on the coating of the sampled particles, *Atmos. Meas. Tech.*, 10, 1043–1059, <https://doi.org/10.5194/amt-10-1043-2017>, 2017.
- 645 Drinovec, L., Močnik, G., Zotter, P., Prévôt, A. S. H., Ruckstuhl, C., Coz, E., Rupakheti, M., Sciare, J., Müller, T., Wiedensohler, A., and Hansen, A. D. A.: The "dual-spot" Aethalometer: an improved measurement of aerosol black carbon with real-time loading compensation, *Atmos. Meas. Tech.*, 8, 1965-1979, <https://doi.org/10.5194/amt-8-1965-2015>, 2015.
- 650



- Ealo, M., Alastuey, A., Ripoll, A., Pérez, N., Minguillón, M. C., Querol, X., and Pandolfi, M.: Detection of Saharan dust and biomass burning events using near-real-time intensive aerosol optical properties in the north-western Mediterranean, *Atmos. Chem. Phys.*, 16, 12567–12586, <https://doi.org/10.5194/acp-16-12567-2016>, 2016.
- 655 ECAC-report-IN-2015-1-5: [https://www.actris-ecac.eu/files/ECAC-report-IN-2015-1-5\\_the-cyprus-institute\\_TSI3563-1082.pdf](https://www.actris-ecac.eu/files/ECAC-report-IN-2015-1-5_the-cyprus-institute_TSI3563-1082.pdf), last access: 17 June 2019, 2016.
- Engelbrecht, J. P., Moosmüller, H., Pincock, S., Jayanty, R. K. M., Lersch, T., and Casuccio, G.: Technical note: Mineralogical, chemical, morphological, and optical interrelationships of mineral dust re-suspensions, *Atmos. Chem. Phys.*, 16, 10809–10830, <https://doi.org/10.5194/acp-16-10809-2016>, 2016.
- 660 European Commission, Establishing guidelines for demonstration and subtraction of exceedances attributable to natural sources under the Directive 2008/50/EC on ambient air quality and cleaner air for Europe, SEC(2011) 208 final, Brussels, 15.02.2011, [http://ec.europa.eu/environment/air/quality/legislation/pdf/sec\\_2011\\_0208.pdf](http://ec.europa.eu/environment/air/quality/legislation/pdf/sec_2011_0208.pdf), accessed 13 May 2019.
- 665 European Committee for Standardisation, EN 16909:2017 Ambient air - Measurement of elemental carbon (EC) and organic carbon (OC) collected on filters, CEN, Brussels, 2017.
- European Committee for Standardisation, EN 16913:2017 Ambient Air—Standard Method for the Measurement of NO<sub>3</sub><sup>-</sup>, SO<sub>4</sub><sup>2-</sup>, Cl<sup>-</sup>, NH<sub>4</sub><sup>+</sup>, Na<sup>+</sup>, K<sup>+</sup>, Mg<sup>2+</sup>, Ca<sup>2+</sup> in PM<sub>2.5</sub> as deposited on filters, CEN, Brussels, 2017.
- 670 Fang, G.C., Kuo, Y.C. and Zhuang, Y.J.: Source Analysis of Trace Metal Pollution Received at Harbor, Airport and Farmland Locations in Central Taiwan, *Aerosol Air Qual. Res.*, 15, 1774–1786, <https://doi.org/10.4209/aaqr.2014.12.0314>, 2015.
- Fialho, P., Cerqueira, M., Pio, C., Cardoso, J., Nunes, T., Custódio, D., Alves, C., Almeida, S. M., Almeida-Silva, M., Reis, M., Rocha, F.: The application of a multi-wavelength Aethalometer to estimate iron dust and black carbon concentrations in the marine boundary layer of Cape Verde, *Atmos. Environ.*, 97, 136–143, <https://doi.org/10.1016/j.atmosenv.2014.08.008>, 2014.
- 675 Fialho, P., Freitas, M.C., Barata, F., Vieira, B., Hansen, A.D.A., Honrath, R.E.: The Aethalometer calibration and determination of iron concentration in dust aerosols, *J. Aerosol Sci.*, 37, 1497–1506. <http://dx.doi.org/10.1016/j.jaerosci.2006.03.002>, 2006.
- 680 Fialho, P., Hansen, A.D.A., Honrath, R.E.: Absorption coefficients by aerosols in remote areas: a new approach to decouple dust and black carbon absorption coefficients using seven-wavelength Aethalometer data, *J. Aerosol Sci.*, 36, 267–282, <http://dx.doi.org/10.1016/j.jaerosci.2004.09.004>, 2005.
- Formenti, P., Rajot, J. L., Desboeufs, K., Caquineau, S., Chevaillier, S., Nava, S., Gaudichet, A., Journet, E., Triquet, S., Alfaro, S., Chiari, M., Haywood, J., Coe, H. and Highwood, E.: Regional variability of the composition of mineral dust from western Africa: Results from the AMMA SOP0/DABEX and DODO field campaigns, *J. Geophys. Res.*, 113, D00C13, doi:10.1029/2008JD009903, 2008.
- Greilinger, M., Schauer, G., Baumann-Stanzer, K., Skomorowski, P., Schöner, W. and Kasper-Giebl, A.: Contribution of Saharan Dust to Ion Deposition Loads of High Alpine Snow Packs in Austria (1987–2017). *Front. Earth Sci.* 6:126. <https://doi.org/10.3389/feart.2018.00126>, 2018.
- 690 Guieu, C., Lo`ye-Pilot, M.-D., Ridame, C., and Thomas, C.: Chemical Characterization of the Saharan dust end-member: Some biogeochemical implications for the Western Mediterranean sea, *J. Geophys. Res.*, 107, doi:10.1029/2001JD000582, 2002.
- Hand, V. L., Capes, G., Vaughan, D. J., Formenti, P., Haywood, J. M. and Coe, H.: Evidence of internal mixing of African dust and biomass burning particles by individual particle analysis using electron beam techniques, *J. Geophys. Res.*, 115, D13301, doi:10.1029/2009JD012938, 2010.
- 695 Herbert F., Dune, Chilton books, Philadelphia, 1965.
- Jeong, C.-H., Wang, J. M., and Evans, G. J.: Source Apportionment of Urban Particulate Matter using Hourly Resolved Trace Metals, Organics, and Inorganic Aerosol Components, *Atmos. Chem. Phys. Discuss.*, <https://doi.org/10.5194/acp-2016-189>, 2016.
- 700 Linke, C., Möhler, O., Veres, A., Mohácsi, Á., Bozóki, Z., Szabó, G., and Schnaiter, M.: Optical properties and mineralogical composition of different Saharan mineral dust samples: a laboratory study, *Atmos. Chem. Phys.*, 6, 3315–3323, <https://doi.org/10.5194/acp-6-3315-2006>, 2006.
- Mamali, D., Marinou, E., Sciare, J., Pikridas, M., Kokkalis, P., Kottas, M., Biniotoglou, I., Tsekeri, A., Keleshis, C., Engemann, R., Baars, H., Ansmann, A., Amiridis, V., Russchenberg, H., and Biskos, G.: Vertical profiles of aerosol mass concentration derived by unmanned airborne in situ and remote sensing instruments during dust events, *Atmos. Meas. Tech.*, 11, 2897–2910, <https://doi.org/10.5194/amt-11-2897-2018>, 2018.
- 705 Mamouri, R. E., Ansmann, A., Nisantzi, A., Kokkalis, P., Schwarz, A., and Hadjimitsis, D.: Low Arabian extinction-to-backscatter ratio, *Geophys. Res. Lett.*, 40, 4762–4766, doi:10.1002/grl.50898, 2013.



- 710 Marinou, E., Tesche, M., Nenes, A., Ansmann, A., Schrod, J., Mamali, D., Tsekeri, A., Pikridas, M., Baars, H., Engelmann, R., Voudouri, K.-A., Solomos, S., Sciare, J., Groß, S., Ewald, F., and Amiridis, V.: Retrieval of ice-nucleating particle concentrations from lidar observations and comparison with UAV in situ measurements, *Atmos. Chem. Phys.*, 19, 11315–11342, <https://doi.org/10.5194/acp-19-11315-2019>, 2019.
- 715 Middleton, N., Yiallourous, P., Kleanthous, S., Kolokotroni, O., Schwartz, J., Dockery, D. W., Demokritou, P. and Koutrakis, P.: A 10-year time-series analysis of respiratory and cardiovascular morbidity in Nicosia, Cyprus: the effect of short-term changes in air pollution and dust storms, *Environ. Health*, 7, 39, <https://doi.org/10.1186/1476-069X-7-39>, 2008.
- 720 Myhre, G., Shindell, D., Bréon, F.-M., Collins, W., Fuglestvedt, J., Huang, J., Koch, D., Lamarque, J.-F., Lee, D., Mendoza, B., Nakajima, T., Robock, A., Stephens, G., Takemura, T. and Zhang, H.: Anthropogenic and Natural Radiative Forcing. In: *Climate Change 2013: The Physical Science Basis. Contribution of Working Group I to the Fifth Assessment Report of the Intergovernmental Panel on Climate Change* [Stocker, T.F., D. Qin, G.-K. Plattner, M. Tignor, S.K. Allen, J. Boschung, A. Nauels, Y. Xia, V. Bex and P.M. Midgley (eds.)]. Cambridge University Press, Cambridge, United Kingdom and New York, NY, USA, 2013.
- 725 Pandolfi, M., Cusack, M., Alastuey, A., and Querol, X.: Variability of aerosol optical properties in the Western Mediterranean Basin, *Atmos. Chem. Phys.*, 11, 8189–8203, <https://doi.org/10.5194/acp-11-8189-2011>, 2011.
- Pandolfi, M., Ripoll, A., Querol, X., and Alastuey, A.: Climatology of aerosol optical properties and black carbon mass absorption cross section at a remote high-altitude site in the western Mediterranean Basin, *Atmos. Chem. Phys.*, 14, 6443–6460, <https://doi.org/10.5194/acp-14-6443-2014>, 2014.
- 730 Park, S. S., Hansen, A. D. A., and Cho, Y.: Measurement of real time black carbon for investigating spot loading effects of Aethalometer data, *Atmos. Environ.*, 11, 1449–1455, doi:10.1016/j.atmosenv.2010.01.025, 2010.
- Perez, L., Tobias, A., Querol, X., Pey, J., Alastuey, A., Diaz, J., Sunyer, J.: Saharan dust, particulate matter and cause-specific mortality: A case–crossover study in Barcelona (Spain), *Environ. International* (48) 150–155, <https://doi.org/10.1016/j.envint.2012.07.001>, 2012.
- 735 Phillips-Smith, C., Jeong, C.-H., Healy, R. M., Dabek-Zlotorzynska, E., Celo, V., Brook, J. R., and Evans, G.: Sources of particulate matter components in the Athabasca oil sands region: investigation through a comparison of trace element measurement methodologies, *Atmos. Chem. Phys.*, 17, 9435–9449, <https://doi.org/10.5194/acp-17-9435-2017>, 2017.
- 740 Pikridas, M., Bezantakos, S., Močnik, G., Keleshis, C., Brechtel, F., Stavroulas, I., Demetriades, G., Antoniou, P., Vouterakos, P., Argyrides, M., Liakakou, E., Drinovec, L., Marinou, E., Amiridis, V., Vrekoussis, M., Mihalopoulos, N., and Sciare, J.: On-flight intercomparison of three miniature aerosol absorption sensors using unmanned aerial systems (UASs), *Atmos. Meas. Tech.*, 12, 6425–6447, <https://doi.org/10.5194/amt-12-6425-2019>, 2019.
- 745 Pikridas, M., Vrekoussis, M., Sciare, J., Kleanthous, S., Vasiliadou, E., Kizas, C., Savvides, C., and Mihalopoulos, N.: Spatial and temporal (short and long-term) variability of submicron, fine and sub-10  $\mu\text{m}$  particulate matter (PM<sub>1</sub>, PM<sub>2.5</sub>, PM<sub>10</sub>) in Cyprus, *Atmos. Environ.*, 191, 79–93, <https://doi.org/10.1016/j.atmosenv.2018.07.048>, 2018.
- Poulakis, E., Theodosi, C., Bressi, M., Sciare, J., Gheri, V., and Mihalopoulos, N.: Airborne mineral components and trace metals in Paris region: spatial and temporal variability. *Environ Sci Pollut R*, 22(19), 14663–14672, 2015.
- 750 Rodríguez, S., Querol, X., Alastuey, A., Kallos, G., Kakaliagou, O.: Saharan dust contributions to PM<sub>10</sub> and TSP levels in Southern and Eastern Spain, *Atmos. Environ.* (35), 2433–2447, [https://doi.org/10.1016/S1352-2310\(00\)00496-9](https://doi.org/10.1016/S1352-2310(00)00496-9), 2001.
- 755 Schauer, G., Kasper-Giebl, A., and Močnik, G. Increased PM concentrations during a combined wildfire and Saharan dust event observed at high-altitude sonnblick observatory, Austria. *Aerosol Air Qual. Res.* 16, 542–554. doi: 10.4209/aaqr.2015.05.0337, 2016.
- Schrod, J., Weber, D., Drücke, J., Keleshis, C., Pikridas, M., Ebert, M., Cvetković, B., Nickovic, S., Marinou, E., Baars, H., Ansmann, A., Vrekoussis, M., Mihalopoulos, N., Sciare, J., Curtius, J., and Bingemer, H. G.: Ice nucleating particles over the Eastern Mediterranean measured by unmanned aircraft systems, *Atmos. Chem. Phys.*, 17, 4817–4835, <https://doi.org/10.5194/acp-17-4817-2017>, 2017.
- 760 Sciare, J., D'Argouges, O., Esteve, R. S., Gaimoz, C., Dolgorouky, C., Bonnaire, N., Favez, O., Bonsang, B., and Gros, V.: Large contribution of water insoluble secondary organic aerosols in the region of Paris (France) during wintertime, *J. Geophys. Res.*, 116, D22203, doi:10.1029/2011JD015756, 2011.
- Sciare, J., Oikonomou, K., Cachier, H., Mihalopoulos, N., Andreae, M. O., Maenhaut, W., and Sarda-Estève, R.: Aerosol mass closure and reconstruction of the light scattering coefficient over the Eastern Mediterranean



- 765 Sea during the MINOS campaign, *Atmos. Chem. Phys.*, 5, 2253–2265, <https://doi.org/10.5194/acp-5-2253-2005>, 2005.
- Sioutas, C., Koutrakis, P., Burton, R.M.: Development of a low cutpoint slit virtual impactor for sampling ambient fine particles, *Journal Aerosol Sci.*, 25, 1321–1330, [https://doi.org/10.1016/0021-8502\(94\)90128-7](https://doi.org/10.1016/0021-8502(94)90128-7), 1994.
- 770 Sokolik, I. and Toon, O.: Incorporation of mineralogical composition into models of the radiative properties of mineral aerosol from UV to IR wavelengths, *J. Geophys. Res.*, 104, 9423–9444, 1999.
- Valenzuela, A., Olmo, F. J., Lyamani, H., Antón, M., Titos, G., Cazorla, A., and Alados-Arboledas, L.: Aerosol scattering and absorption Angström exponents as indicators of dust and dust-free days over Granada (Spain), *Atmos. Res.*, 154, 1–13, <https://doi.org/10.1016/j.atmosres.2014.10.015>, 2015.
- 775 Viana, M., Salvador, P., Artíñano, B., Querol, X., Alastuey, A., Pey, J., Latz, A. J., Cabañas, M., Moreno, T., Dos Santos, S. G., Herce, M. D., Hernández, P. D., García D. R., and Fernández-Patier, R.: Assessing the Performance of Methods to Detect and Quantify African Dust in Airborne Particulates, *Environ. Sci. Tech.* 44, 8814–8820, <https://doi.org/10.1021/es1022625>, 2010.
- 780 Visser, S., Slowik, J. G., Furger, M., Zotter, P., Bukowiecki, N., Canonaco, F., Flechsig, U., Appel, K., Green, D. C., Tremper, A. H., Young, D. E., Williams, P. I., Allan, J. D., Coe, H., Williams, L. R., Mohr, C., Xu, L., Ng, N. L., Nemitz, E., Barlow, J. F., Haliou, C. H., Fleming, Z. L., Baltensperger, U., and Prévôt, A. S. H.: Advanced source apportionment of size-resolved trace elements at multiple sites in London during winter, *Atmos. Chem. Phys.*, 15, 11291–11309, <https://doi.org/10.5194/acp-15-11291-2015>, 2015a.
- 785 Vrekoussis, M., Liakakou, E., Koçak, M., Kubilay, N., Oikonomou, K., Sciare, J., Mihalopoulos, N.: Seasonal variability of optical properties of aerosols in the Eastern Mediterranean, *Atmo. Environ.* 39, 7083–7094, <https://doi.org/10.1016/j.atmosenv.2005.08.011>, 2005.
- Weingartner, E., Saathoff, H., Schnaiter, M., Streit, N., Bitnar, B., and Baltensperger, U.: Absorption of light by soot particles: determination of the absorption coefficient by means of aethalometers, *J. Aerosol Sci.*, 34, 1445–1463, [doi:10.1016/S0021-8502\(03\)00359-8](https://doi.org/10.1016/S0021-8502(03)00359-8), 2003.
- 790 WHO, Workshop: Evaluating the short-term health effects of desert and anthropogenic dust, 29 October 2018, Geneva, WHO.
- WMO, Report No. 227: WMO/GAW Aerosol Measurement Procedures, Guidelines and Recommendations, 2<sup>nd</sup> Edition, 2016, Geneva, WMO.
- 795 Zhang, X. Y., Wang, Y. Q., Zhang, X. C., Guo, W., Niu, T., Gong, S. L., Yin, Y., Zhao, P., Jin, J. L., and Yu M.: Aerosol monitoring at multiple locations in China: contributions of EC and dust to aerosol light absorption, *Tellus B: Chemical and Physical Meteorology*, 60:4, 647–656, [doi:10.1111/j.1600-0889.2008.00359.x](https://doi.org/10.1111/j.1600-0889.2008.00359.x), 2008.